Journal of Alloys and Compounds 486 (2009) 278–283

Contents lists available at ScienceDirect

Journal of Alloys and Compounds

journal homepage: www.elsevier.com/locate/jallcom

TiCrV hydrogen storage alloy studied by positron annihilation spectroscopy

A. Kawasuso[a,*], H. Arashima[b], M. Maekawa[a], H. Itoh[b], T. Kabutomori[b]

[a] ASRC, Japan Atomic Energy Agency, 1233 Takasaki, Gunma 370-1292, Japan
[b] MRL, The Japan Steel Works, Ltd., 4 Chatsumachi, Muroran, Hokkaido 051-8505, Japan

ARTICLE INFO

Article history:
Received 7 April 2009
Received in revised form 18 June 2009
Accepted 19 June 2009
Available online 26 June 2009

Keywords:
Hydrogen absorbing materials
Metal hydrides
Crystal structure
Positron spectroscopy
X-ray diffraction

ABSTRACT

We have studied the structural changes of $Ti_{24}Cr_{36}V_{40}$ alloy prepared by arc-melting using positron annihilation spectroscopy and X-ray diffraction (XRD) as functions of the number of hydrogen pressure swing cycles and degassing temperature. As the hydrogen storage capacity decreased with the number of pressure swing cycles, both positron lifetime and XRD peak width increased. Upon hydriding, the crystal structure changed from bcc to bct with increased lattice constants. The increase in positron lifetime is due to the volume expansion caused by hydride formation. After degassing at 500 °C, the hydrogen storage capacity recovered to 95% of the initial level, and the XRD peak width and the lattice constants nearly completely returned to their initial values. However, the positron lifetime was still longer than the initial level suggesting the survival of dislocations. The degradation of hydrogen storage capacity is probably caused by both hydride formation and the generation of dislocations.

1. Introduction

To realize hydrogen fuel cell vehicles, the rechargeable hydrogen storage capacity of the storage material should be improved to more than 4 mass% [1]. Vanadium is known to be one of metals that satisfies the above condition. However, the use of vanadium is not well suited in light of cost performance. Recently, a solid solution alloy of Ti–Cr–V is extensively studied as a substitutional material of vanadium. By adjusting the lattice parameter to that of pure vanadium, this alloy exhibits relatively high hydrogen storage capacity compared to the other alloys [2–5]. If this alloy is prepared with high vanadium content (i.e., more than 80%), the rechargeable hydrogen storage capacity retains 99% of its initial level even after several hundred pressure swing cycles [6–8]. However, when the vanadium content is less than 40%, the rechargeable hydrogen storage capacity decreases dramatically following pressure swing cycles. Therefore, improving the durability of the storage material against pressure swing cycles at low vanadium content is an important issue.

Many comprehensive studies have been performed to improve the degradation of hydrogen storage capacity at low vanadium content. Melt-quenching [9], floating-zone-melting [10] and mechanical pre-pulverization [11–13] have been proposed as effective means of enhancing rechargeable hydrogen storage capacity. From a fundamental viewpoint, stable hydride formation, phase dissociation, strain accumulation, defect formation and surface contamination are regarded as the causes of degradation [14,15]. That is, the above phenomena result in the reduction in the number of hydrogen occupation sites, the impediment of hydrogen motion and the suppression of the dissociation reaction of hydrogen molecules. As for the defect formation, many dislocations are introduced because of the repeated volume expansions and contractions. Excess vacancies are also expected to form because of the reduction of the formation energy due to hydriding [16]. These defects may trap hydrogen to degrade the rechargeable storage capacity. Vacancies also degrade the material itself through the formation of voids and the enhancement of phase segregation. Thus, to improve the hydrogen storage capacity, it is important to clarify the structural changes due to hydriding and to incorporate this knowledge into the casting process of hydrogen storage alloys.

Positron annihilation spectroscopy is a powerful tool for detecting vacancy defects and dislocations in solid materials, and several studies have been carried out on hydrogen storage alloys. In AB_5 and AB_2 type alloys, the positron lifetime was found to increase during hydriding [17,18]. The positron lifetime was further prolonged upon thermal annealing after hydriding. Based on these findings, vacancy defects are thought to form during hydriding. An increase in positron lifetime was also observed in hydrogen-loaded Nb [19,20]. Through a comparison with theoretical calculations, the increased positron lifetime was attributed to the formation of vacancy-hydrogen complexes. It is intriguing to examine whether vacancy defects are also formed in the Ti–Cr–V ternary alloy.

In this paper, using positron annihilation spectroscopy and X-ray diffraction (XRD), we investigated the microscopic structural changes of Ti–Cr–V alloys prepared by the arc-melting method upon hydriding and high-temperature degassing.

* Corresponding author. Tel.: +81 27 346 9331; fax: +81 27 346 9690.
E-mail address: kawasuso.atsuo@jaea.go.jp (A. Kawasuso).

0925-8388/$ – see front matter © 2009 Elsevier B.V. All rights reserved.
doi:10.1016/j.jallcom.2009.06.125

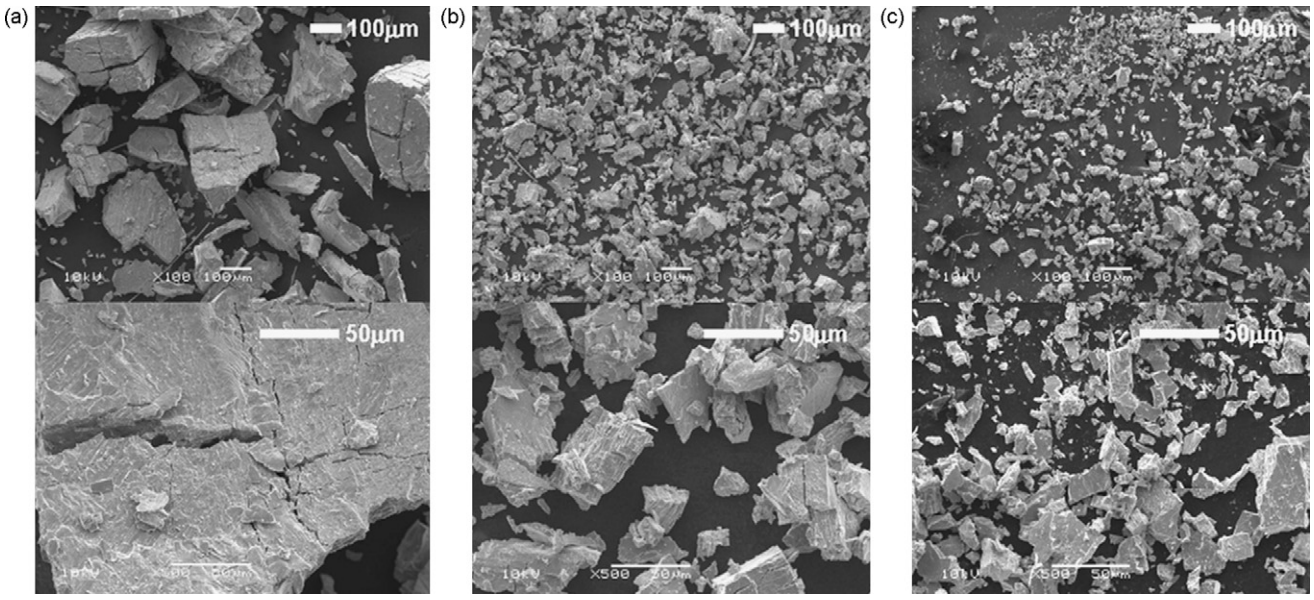

Fig. 1. Secondary electron microscope images of $Ti_{24}Cr_{36}V_{40}$ samples after pressure swing cycles of (a) $N = 1$, (b) $N = 20$ and (c) $N = 1000$.

2. Materials and methods

The Ti–Cr–V alloy samples were prepared by arc-melting under an argon atmosphere in a water-cooled Cu crucible. The target composition was $Ti_{24}Cr_{36}V_{40}$ or $Ti_8Cr_{12}V_{80}$. The ingots were annealed at 1400 °C in order to homogenize the material. Subsequently, one hydrogen activation process was carried out under a hydrogen pressure of 4.5 MPa at room temperature following degassing treatment at 100 °C. After the activation process, one sample was pulverized mechanically to reduce the particle size to less than 20 μm. Pressure composition isotherms (PCT) were measured in a conventional Sieverts-type apparatus at room temperature. From the PCT curves, the hydrogen storage capacity and residual amount of hydrogen in the samples were determined. Here, 1 mass% of hydrogen corresponds to 111.2 cc/g and a hydrogen-to-metal ratio (H/M) of 0.502. Upon one activation cycle, the ingots were pulverized as shown in the secondary electron microscope images in Fig. 1a, and the particle size was decreased to less than 50 μm by subsequent cycles (Fig. 1b and c). After the pressure swing cycles, the samples were degassed in a vacuum for 1 h at temperatures up to 500 °C.

Powder XRD analysis using Cu-Kα radiation was performed to determine the crystal structure and lattice constants. The dislocation density was determined from transmission electron microscopy (TEM) observations using a JEM-2010 operated at 200 kV. The pulverized samples were put into small cases with titanium windows (2 μm thick). Positron lifetime measurements were performed using a conventional spectrometer with a time resolution of 200 ps and a sodium-22 source of 370 kBq. The lifetime spectra were analyzed using the PATFIT-88 program [21]. Doppler broadening of annihilation radiation (DBAR) measurements were also performed to investigate the physical and chemical changes at the positron annihilation sites. The energy resolution was approximately 1 keV.

3. Calculation of positron annihilation characteristics

To interpret the experimental positron lifetime and DBAR spectrum, theoretical calculations were carried out. Positron lifetime was calculated based on the atomic superposition method developed by Puska et al. [22] with the Borónski–Niemnen enhancement factor [23]. This calculation scheme is well established for a number of materials. A supercell including 60(20) Ti atoms, 90(30) Cr atoms and 100(200) V atoms corresponding to the $5 \times 5 \times 5$ bcc conventional unit cell was constructed as the $Ti_{24}Cr_{36}V_{40}$ ($Ti_8Cr_{12}V_{80}$) bulk alloy. The lattice constant was adjusted using the experimental values obtained from the XRD measurement. The atomic sites for individual elements were determined by generating random numbers. For the calculation of vacancies, relevant atoms were removed. It is reported that hydrogen atoms occupy the tetrahedral site when its amount is high, while octahedral site when low content [24,25]. Hence, to simulate the hydride states, hydrogen atoms were randomly distributed to the octahedral or tetrahedral sites. The occupation fraction of these sites depended on the experimentally determined H/M ratio.

The DBAR spectra were calculated within the local density approximation [22]. The valence electron wavefunctions were calculated based on the projector augmented-wave (PAW) method [26] using the ABINIT4.6.4 code [27]. The potentials and projectors were generated using the ATOMPAW code [28]. The valence electron configurations were $3s^2 2p^6 3d^2 4s^2$, $3s^2 2p^6 3d^3 4s^2$ and $3s^2 2p^6 3d^5 4s^1$ for Ti, V and Cr atoms, respectively. A supercell including 4 Ti, 6 Cr and 6 V atoms with a $2 \times 2 \times 2$ conventional bcc or bct unit cell was constructed as the $Ti_{24}Cr_{36}V_{40}$ bulk alloy. The lattice constants and the manner of hydrogen distribution were the same as the above lifetime calculation. The k-point mesh was $2 \times 2 \times 2$. The cut-off energy of the plane wave basis set was 60 Ryd. The core electron wavefunctions were represented by the Slater function parameterized by Clementi and Roetti [29]. A self-consistent positron wavefunction was calculated based on the two-component density functional theory in order to minimize the energy functional [23]. The Borónski–Nieminen enhancement factor was adopted. The DBAR spectra were obtained by convoluting one-dimensional angular correlation of the annihilation radiation spectra obtained from the momentum density with the Gaussian resolution function having a half width of $3.92 \times 10^{-3}\, m_0 c$.

4. Results and discussion

4.1. Degradation of hydrogen storage capacity

4.1.1. $Ti_{24}Cr_{36}V_{40}$

Fig. 2 shows the rechargeable hydrogen storage capacity normalized to its initial value as a function of the number of pressure swing cycles N. The rechargeable hydrogen storage capacity decreases rapidly following the initial pressure swing cycle and maintains a constant value up to $N = 1000$.

In Fig. 2, the average positron lifetime and the full width at half maximum (FWHM) of the XRD (1 1 0) peak after degassing at 100 °C are also plotted. The numerical data are listed in Table 1. The (1 1 0) peak width increases up to $N = 20$ and then maintains a nearly constant value up to $N = 1000$. In the XRD rocking curve, new peaks indicating the change of crystal structure from bcc to

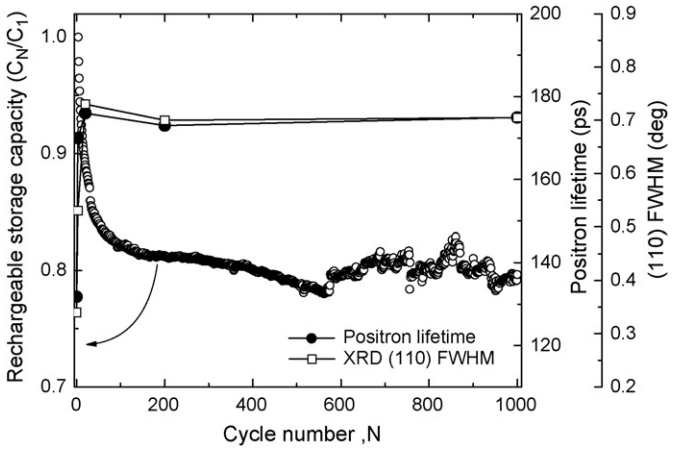

Fig. 2. Rechargeable hydrogen storage capacity, positron lifetime and XRD (1 1 0) peak width (FWHM) obtained for the $Ti_{24}Cr_{36}V_{40}$ sample as a function of the number of pressure swing cycles. After each cycle, samples were subjected to degassing treatment at 100 °C. The rest hydrogen amount after each cycle is approximately 100–110 cc/g.

bct appeared at $N > 20$ cycles. As listed in Table 2, before hydriding, the lattice constant was $a = 3.03$ Å, whereas after the pressure swing cycle of $N = 50$, the lattice constants were $a = 3.092$ Å and $c = 3.227$ Å. Thus, the unit cell volume increases by approximately 10% due to hydriding. Even after degassing at room temperature, the volume expansion remains.

In the positron lifetime measurements before hydriding, only one short-lived component ($\tau = 132$ ps) was obtained. This is 12 ps longer than the bulk lifetime of $Ti_{24}Cr_{36}V_{40}$ calculated using the atomic superposition method as listed in Table 3. The positron

Table 3
Calculated positron lifetimes for bcc Ti24Cr36V40 bulk, monovacancies and bct Ti24Cr36V40 bulk with and without hydrogen incorporation.

State	Positron lifetime	
bcc $Ti_{24}Cr_{36}V_{40}$		
Bulk (a = 3.03 Å)	120 ps	
Ti vacancy	205 ps	
Cr vacancy	207 ps	
V vacancy	206 ps	
bct $Ti_{24}Cr_{36}V_{40}$		
Bulk (a = 3.072 Å, c = 3.205 Å, H/M = 0.75)[a]	O-site H	T-site H
	164 ps	170 ps
Bulk (a = 3.072 Å, c = 3.205 Å, H/M = 0)	179 ps	
bct $Ti_8Cr_{12}V_{80}$		
Bulk (a = 3.027 Å, c = 3.281 Å, H/M = 0.55)[a]	O-site H	T-site H
	185 ps	187 ps
Bulk (a = 3.027 Å, c = 3.281 Å, H/M = 0)	194 ps	

[a] These calculation conditions correspond to the states after the pressure swing cycles of $N = 50$ and 200 and degassing at room temperature and 100 °C for $Ti_{24}Cr_{36}V_{40}$ and $Ti_8Cr_{12}V_{80}$, respectively.

Table 1
Positron lifetimes (τ) and XRD (1 1 0) peak widths (FWHM) measured in this study.

Cycle number	Degassing temperature	$Ti_{24}Cr_{36}V_{40}$		$Ti_{24}Cr_{36}V_{40}$ (pre-pulverized)		$Ti_8Cr_{12}V_{80}$	
		τ	FWHM	τ	FWHM	τ	FWHM
Pressure swing cycle dependence							
0	–	132 ps	0.34 deg	133 ps	0.25 deg	128 ps	0.41 deg
150 cc/g	100 °C	142 ps	0.27 deg	144 ps	0.30 deg	–	–
1	100 °C	165 ps	0.36 deg	167 ps	0.44 deg	–	–
3	100 °C	170 ps	0.53 deg	–	–	164 ps	0.39 deg
20	100 °C	176 ps	0.73 deg	–	–	–	–
200	100 °C	173 ps	0.70 deg	–	–	165 ps	0.56 deg
1000	100 °C	175 ps	0.71 deg	–	–	–	–
Degassing temperature dependence[a]							
0	–	132 ps	0.68 deg				
50	–	172 ps	1.57 deg	–	–	–	–
50	26 °C	171 ps	1.47 deg	–	–	–	–
50	100 °C	169 ps	1.28 deg	–	–	–	–
50	200 °C	166 ps	1.18 deg	–	–	–	–
50	300 °C	162 ps	0.89 deg	–	–	–	–
50	400 °C	161 ps	0.86 deg	–	–	–	–
50	500 °C	157 ps	0.67 deg	–	–	–	–

[a] Peak widths were broadened due to the stronger source of the XRD apparatus in this experiment. However, there is no fundamental problem as long as the relative values are compared.

Table 2
Pressure swing cycles, degassing temperatures, crystal structures, lattice constants, unit cell volumes and rest hydrogen amounts obtained for $Ti_{24}Cr_{36}V_{40}$ and $Ti_8Cr_{12}V_{80}$ samples.

Cycle number	Degassing temperature	Structure	a-Axis	c-Axis	Unit cell volume	Rest hydrogen amount
$Ti_{24}Cr_{36}V_{40}$						
0	–	bcc	3.030 Å	–	27.818 Å^3	–
50	–	bct	3.092 Å	3.227 Å	30.852 Å^3	191 cc/g
50	26 °C	bct	3.072 Å	3.205 Å	30.246 Å^3	164 cc/g
50	100 °C	bct	3.056 Å	3.181 Å	29.708 Å^3	119 cc/g
50	200 °C	bcc	3.050 Å	–	28.373 Å^3	70 cc/g
50	300 °C	bcc	3.032 Å	–	27.873 Å^3	31 cc/g
50	400 °C	bcc	3.029 Å	–	27.791 Å^3	21 cc/g
50	500 °C	bcc	3.030 Å	–	27.818 Å^3	8 cc/g
$Ti_8Cr_{12}V_{80}$						
0	–	bcc	3.029 Å	–	27.791 Å^3	–
3	100 °C	bct	3.027 Å	3.281 Å	30.054 Å^3	–
200	100 °C	bct	3.027 Å	3.280 Å	30.054 Å^3	110 cc/g

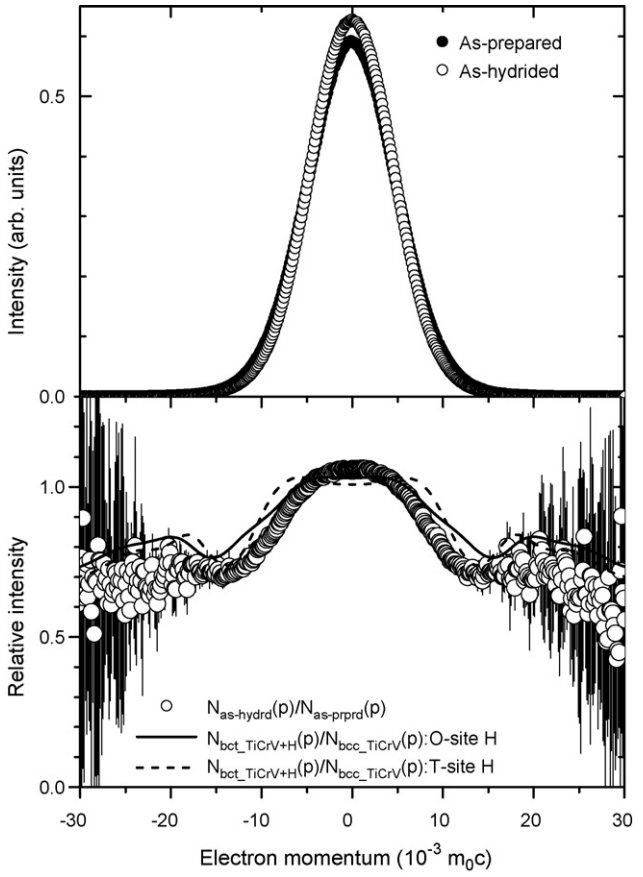

Fig. 3. Upper panel shows the DBAR spectra obtained for the as-prepared $Ti_{24}Cr_{36}V_{40}$ sample (filled circle: $N_{as\text{-}prprd}(p)$) and that after pressure swing cycles of $N = 50$ and subsequent degassing at room temperature (open circle: $N_{as\text{-}hydrd}(p)$). Lower panel shows their difference (open circles: $N_{as\text{-}hydrd}(p)/N_{as\text{-}prprd}(p)$). Solid and broken lines indicate the theoretical DBAR spectra for bct $Ti_{24}Cr_{36}V_{40}$ crystals calculated from the experimentally determined volume expansion and residual hydrogen amount. Hydrogen atoms are assumed to occupy the octahedral site (solid line) and the tetrahedral site (broken line). The spectra are differentiated by that for the perfect bcc $Ti_{24}Cr_{36}V_{40}$ crystal ($N_{bct.TiCrV+H}(p)/N_{bcc.TiCrV}(p)$).

lifetimes related to dislocations may be prolonged by less than 10 ps compared to the bulk lifetime [30,31]. Thus, before hydriding, positron annihilation occurs in both the perfect lattice region and at residual dislocations. After partial hydriding (150 cc/g), the positron lifetime increases to 142 ps. At $N = 20$, the positron lifetime reaches 176 ps and maintains a constant value up to $N = 1000$. This behavior is quite similar to that of the XRD (1 1 0) peak width. The decomposition of positron lifetime spectra to the bulk and defect components was rather difficult. This suggests that positrons annihilate from one state and/or from different states giving rise to similar positron lifetimes of around 170–180 ps. Fig. 3 shows the DBAR spectrum after pressure swing cycles of $N = 50$ and degassing at room temperature. To highlight the change due to hydriding, the lower panel of Fig. 3 shows the difference between the as-prepared and the hydrided samples. After hydriding, the intensity increases in the low momentum region ($p < 5\ m_0c$). This corresponds to a narrowing of the DBAR spectrum.

Generally, the increasing positron lifetime and the narrowing DBAR spectrum are explained by the presence of vacancy defects and/or the volume expansion of the material itself. To clarify these possibilities, theoretical calculations were carried out considering monovacancies (Ti, Cr and V vacancies), the volume expansion observed by XRD analysis and the residual hydrogen determined from PCT curves. Table 3 lists the results of these calculations. The positron lifetimes for monovacancies were calculated to be

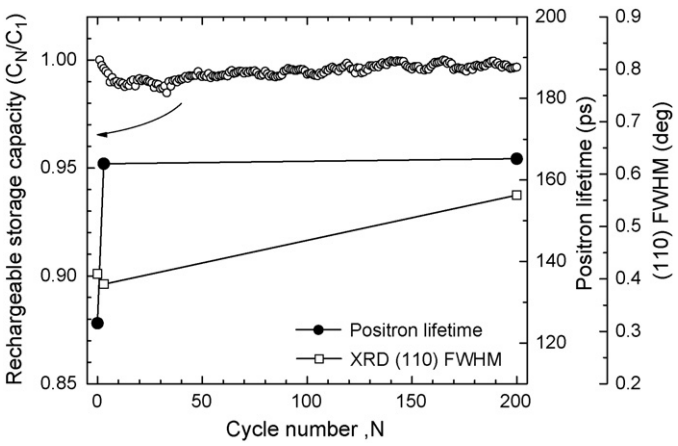

Fig. 4. Rechargeable hydrogen storage capacity, positron lifetime and XRD (1 1 0) peak width (FWHM) obtained for the $Ti_8Cr_{12}V_{80}$ sample as a function of the number of pressure swing cycles. After each cycle, the samples were subjected to degassing treatment at 100 °C. The rest hydrogen amount after each cycle is approximately 100–110 cc/g.

205–207 ps. As mentioned above, such lifetime components were not observed experimentally after hydriding. Thus, the observed positron lifetime of 173 ps is attributed neither to monovacancies nor to vacancy clusters. Contrarily, considering the volume expansion, the positron lifetime is calculated to be 179 ps. Even adding hydrogen, the lifetime is still 164–170 ps. The calculated lifetime of 164–179 ps is in good agreement with the experimental positron lifetime observed after pressure swing cycles of $N > 20$. The solid and broken lines in Fig. 3 show the calculated DBAR spectra considering the volume expansion and residual hydrogen to the octahedral site and tetrahedral site, respectively. The experimental spectrum agrees well with the calculations. Thus, the increase in the positron lifetime and the narrowing of the DBAR spectrum are well explained by the volume expansion due to hydriding. Probably, hydrogen atoms occupy both the tetrahedral and the octahedral sites.

The thermal equilibrium vacancy concentrations in some transition metals are reported to increase considerably upon hydrogen absorption [16]. The increase in positron lifetime observed for AB_5 type metals is also explained by the formation of vacancies [17]. Contrarily, the above results imply that in the case of the Ti–Cr–V alloy, the formation of vacancies due to hydrogen storage is unlikely. The degradation of hydrogen storage capacity was inferred to be due to the formation of stable hydride phases and/or the introduction of dislocations. Considering the fact that volume expansion occurs with the formation of stable hydrides, the degradation of hydrogen storage capacity is dominated by the decrease of hydrogen trapping sites in the crystal.

4.1.2. $Ti_8Cr_{12}V_{80}$

Fig. 4 shows the rechargeable hydrogen storage capacity normalized to its initial value of the $Ti_8Cr_{12}V_{80}$ sample as a function of the number of pressure swing cycles. Unlike the case of $Ti_{24}Cr_{36}V_{40}$, the decrease of rechargeable hydrogen storage capacity is less than 1% of the initial value up to $N = 200$ [4]. The XRD (110) peak width (after degassing at 100 °C) moderately increases with N compared to $Ti_{24}Cr_{36}V_{40}$. The positron lifetime (after degassing at 100 °C) increases to 164 ps at $N = 200$. This is also shorter than that of the $Ti_{24}Cr_{36}V_{40}$ sample. However, the crystal structure transformed from the initial bcc structure with $a = 3.029$ Å to an expanded bct structure with $a = 3.027$ Å and $c = 3.280$ Å. The theoretical positron lifetime was calculated to be 185 ps with the above volume expansion and residual hydrogen amount as shown in Table 3. The observed positron lifetime is significantly shorter than the calculated positron lifetime. Positrons probably annihilate in two

well-separated domains. In one domain, the lattice constants more or less remain constant; in the other domain, they do not. The observed positron lifetime may be a weighted average of the two positron lifetimes from these domains. The former domain is probably larger than the latter.

For the $Ti_{24}Cr_{36}V_{40}$ sample, the clear bct structure was confirmed at $N > 50$. The volume expansion occurs in both the *a*- and *c*-axes. While, in the case of $Ti_8Cr_{12}V_{80}$ sample, the stable bct structure appeared with a preferential extension of the *c*-axis in the early stage of pressure swing cycle. It is inferred that the strain accumulation of the $Ti_8Cr_{12}V_{80}$ sample is relatively small since the lattice distortion occurs only in one axis. Probably, after degassing, the lattice distortion is well relaxed when high vanadium content and hence the degradation of hydrogen storage capacity is suppressed.

4.1.3. Effect of pre-pulverization

After one activation treatment, the ingot samples were pulverized as shown in Fig. 1. Such pulverization is caused by hydrogen embrittlement. Accompanying the brittle fracture, many dislocations are generated because of the remaining ductility of the Ti–Cr–V alloy and the stress concentration. Therefore, if the sample is pre-pulverized by mechanical means to have a particle size below that observed after a number of hydriding cycles, for example, less than 20 μm, it is anticipated that the degradation of hydrogen storage capacity arising from embrittlement may be suppressed. A dramatic decrease in dislocation density near the surface of the particles is frequently observed by TEM in the pre-pulverized samples [11]. Also, from the SEM observation, pre-pulverized samples contain few cracks after an appropriate annealing. We thus anticipated that the volume expansion and contraction of the pre-pulverized samples are more or less reducible. The rechargeable hydrogen storage capacity was actually fairly well enhanced by the pre-pulverization. However, in the initial pressure swing cycle, it decreases to the similar level as the case without pulverization.

The positron lifetime of the pre-pulverized $Ti_{24}Cr_{36}V_{40}$ sample was 133 ps after annealing at 1000 °C. The positron lifetime increased to 144 ps after partial hydriding (150 cc/g) and to 167 ps after full hydriding as listed in Table 1. This tendency is nearly the same as that observed for the samples without pre-pulverization. Therefore, even in the pre-pulverized sample, the volume expansion originating from stable hydride formation and/or the hardening due to the introduction of dislocations occurs and results in the degradation of the desorption amount. Possibly, much finer pre-pulverization is needed to improve the rechargeable hydrogen storage capacity.

4.2. Recovery of hydrogen storage capacity

Fig. 5 shows the hydrogen storage capacity, the rechargeable hydrogen storage capacity and the residual hydrogen amount in the sample after pressure swing cycles of $N = 50$ as a function of degassing temperature. With increasing degassing temperature, the residual hydrogen in the sample is gradually desorbed, and hence the hydrogen storage capacity also recovers. The hydrogen storage capacity at 500 °C is 98% of the initial level. However, 8 cc/g of hydrogen still remains. Furthermore, rechargeable hydrogen storage capacity is still 95% of the initial level. For a full recovery, even higher temperature degassing is needed.

Fig. 6 shows the positron lifetime, the lattice constants and the XRD (1 1 0) peak width as a function of degassing temperature. At 300 °C, the lattice constants returned to the initial values before hydriding. The crystal structure transformed from bct to bcc. The (1 1 0) peak width recovered in two steps at 300 °C and 500 °C. These features agree well with the recovery of hydrogen storage capacity shown in Fig. 5. Therefore, the degradation of hydrogen storage capacity is mainly caused by the formation of stable hydrides.

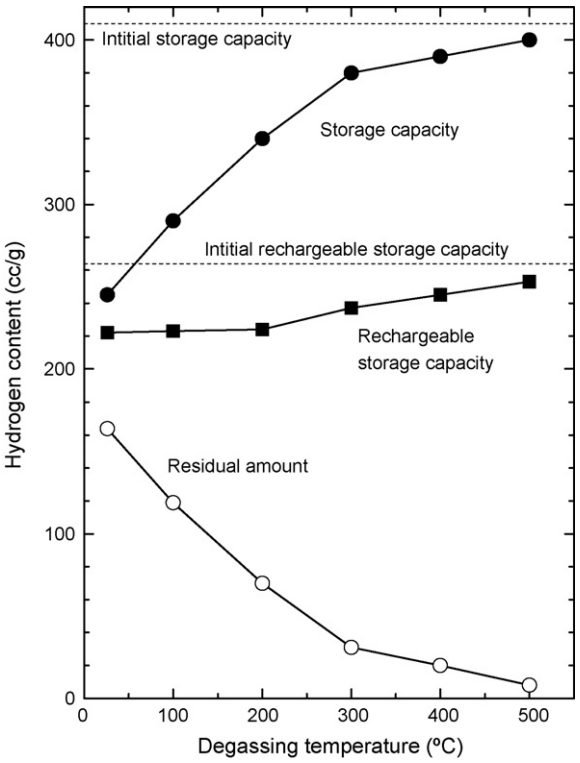

Fig. 5. Hydrogen storage capacity (filled circles), rechargeable hydrogen storage capacity (filled squares) and residual hydrogen amount (open circles) of the $Ti_{24}Cr_{36}V_{40}$ sample after pressure swing cycles of $N = 50$ as a function of degassing temperature. The 'initial' storage capacity and rechargeable hydrogen storage capacity mean their values at $N = 1$. The sum of storage capacity and residual amount is approximately equal to the initial storage capacity.

As seen in Fig. 6, the positron lifetime, like the FWHM of the XRD (1 1 0) peak, also decreases with increasing degassing temperature. For comparison, the positron lifetime calculated using the lattice constants determined by XRD and the residual hydrogen amount from the PCT curve are also plotted. Assuming the recovery of the lattice constants and hydrogen desorption, the positron lifetime should recover to the level before the pressure swing cycle at 300 °C. However, even after degassing at 500 °C, the positron lifetime is still higher than the level before the pressure swing cycle. This means that some lattice defects formed during the pressure swing cycle remains even after the recovery of the lattice constants. Positron lifetime is more sensitive to such lattice defects than the XRD peak width. Since the observed positron lifetime is well below that calculated for monovacancies, dislocations introduced by the volume expansion are probably responsible for positron trapping. In fact, TEM observation revealed that the dislocation density increases from 5×10^8 cm^{-2} to 1×10^{10} cm^{-2} with the pressure swing cycle [11].

According to Shirai et al. [30], the positron lifetime at dislocations in fcc and bcc metals depends on the Burgers vector of the dislocation. For Cu and Au, the positron lifetime at an edge dislocation is approximately 200 ps, while the bulk lifetime is 120 ps. The positron lifetimes for the Frank and Shockley partial dislocations are approximately 180 ps and 160 ps, respectively. Kamimura et al. [31] calculated the positron lifetimes for edge dislocations and vacancies in Fe assuming a realistic lattice relaxation. Their calculation shows that an edge dislocation and even a jog on it act as very shallow positron trapping centers. The positron lifetime increases approximately 10 ps from the bulk lifetime. Therefore, the above positron lifetime observed after the lattice constants return to their initial values is attributed to dislocations. The small amount of hydrogen

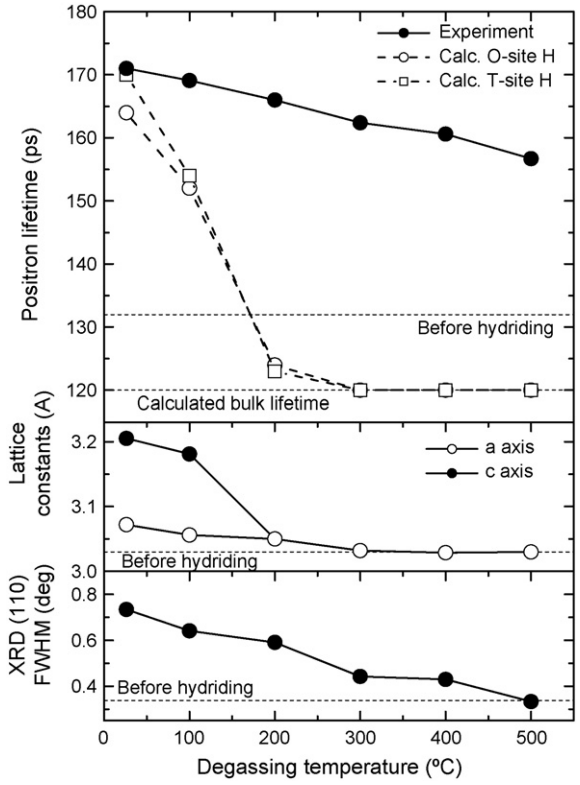

Fig. 6. Positron lifetime (solid circles in top figure), the lattice constants (middle figure), and the XRD (1 1 0) peak width (bottom figure) of the $Ti_{24}Cr_{36}V_{40}$ sample after pressure swing cycles of $N = 50$ as a function of degassing temperature. Positron lifetimes calculated using the crystal structures, the lattice constants and residual hydrogen amount from the experiment are denoted by open circles and squares in the top figure.

remaining after degassing at 500 °C in Fig. 5 may be trapped by dislocations.

5. Conclusion

In this study, we investigated the degradation of the hydrogen storage capacity of $Ti_{24}Cr_{36}V_{40}$ alloy using XRD and positron annihilation methods. These two approaches demonstrated that stable hydride formation, volume expansion and the introduction of dislocations are the main reasons for the degradation of hydrogen storage capacity. From the positron annihilation experiments, the formation of vacancy defects was not confirmed. Although similar structural changes were observed for the $Ti_8Cr_{12}V_{80}$ alloy, these were not significant factors in reducing the hydrogen storage capacity, unlike the case of the $Ti_{24}Cr_{36}V_{40}$ alloy. Pre-pulverization effectively enhanced the hydrogen storage capacity, but finer pulverization is needed for maintaining the rechargeable storage capacity. After degassing at 500 °C, the crystal structure and the lattice constants nearly completely recovered to their initial states. The rechargeable hydrogen storage capacity was 95% of the initial level even after degassing at 500 °C. The prolonged positron lifetime at this temperature indicates the influence of dislocations on the hydrogen storage capacity.

References

[1] D. Mori, K. Hirose, Int. J. Hydrogen Energy 34 (2009) 4569–4574.
[2] T. Kabutomori, H. Takeda, Y. Wakisaka, K. Ohnishi, J. Alloys Compd. 231 (1995) 528–532.
[3] E. Akiba, H. Iba, Intermetallics 6 (1998) 461–470.
[4] S.-W. Cho, C.-S. Han, C.-N. Park, E. Akiba, J. Alloys Compd. 288 (1999) 294–298.
[5] Y. Tominaga, S. Nishimura, T. Amemiya, T. Fuda, T. Tamura, T. Kuriiwa, A. Kamegawa, M. Okada, Mater. Trans. JIM 40 (1999) 871–874.
[6] H. Itoh, H. Arashima, K. Kubo, T. Kabutomori, K. Ohnishi, J. Alloys Compd. 404–406 (2005) 417–420.
[7] Ta. Huang, Z. Wu, B. Xia, Ti. Huang, Mater. Chem. Phys. 93 (2005) 544–547.
[8] T. Huang, Z. Wu, G. Sun, N. Xu, Intermetallics 15 (2007) 593–598.
[9] H. Arashima, K. Hashi, K. Kubo, H. Itoh, T. Kabutomori, K. Ohnishi, J. Jpn. Inst. Met. 70 (2006) 709–714.
[10] H. Arashima, F. Takahashi, T. Ebisawa, H. Itoh, T. Kabutomori, J. Alloys Compd. 356–357 (2003) 405–408.
[11] K. Washio, Y. Munakata, S. Ohnuki, T. Suda, H. Itoh, H. Arashima, K. Kubo, T. Kabutomori, J. Jpn. Inst. Met. 71 (2007) 522–527.
[12] B.K. Singh, G. Shim, S.-W. Cho, Int. J. Hydrogen Energy 32 (2007) 4961–4965.
[13] S.F. Santos, A.L.M. Costa, J.F.R. de Castro, D.S. Dos Santos, F.W.J. Botta, T.T. Ishikawa, J. Metastable Nanocryst. Mater. 20–21 (2004) 291–296.
[14] H. Ho, J. Lee, J. Alloys Compd. 202 (1993) 23–28.
[15] G. Mazzolai, B. Couluzzi, A. Biscarini, F.M. Mazzolai, A. Tuissi, F. Agresti, S. Lo Russo, A. Maddalena, P. Palade, G. Principi, J. Alloys Compd. 466 (2008) 133–139.
[16] Y. Fukai, N. Okuma, Jpn. J. Appl. Phys. 32 (1993) L1256–L1259.
[17] Y. Shirai, H. Araki, T. Mori, W. Nakamura, S. Sakaki, J. Alloys Compd. 330–332 (2002) 125–131.
[18] M. Mizuno, K. Sakaki, H. Araki, Y. Shirai, J. Alloys Compd. 356–357 (2003) 186–190.
[19] J. Čížek, I. Procházka, F. Bečvář, R. Kužel, M. Cieslar, G. Brauer, W. Anwand, R. Kirchheim, A. Pundt, Phys. Rev. B 69 (2004) 224106–224119.
[20] J. Čížek, I. Procházka, S. Danis, M. Cieslar, G. Brauer, W. Anwand, R. Kirchheim, A. Pundt, J. Alloys Compd. 446–447 (2007) 479–483.
[21] P. Kirkegaard, N.J. Pederson, M. Eldrup, PATFIT-88, Riso-M-2704 (1989).
[22] M.J. Puska, R.M. Nieminen, Rev. Mod. Phys. 66 (1994) 841–897.
[23] E. Borónski, R.M. Nieminen, Phys. Rev. B 34 (1986) 3820–3831.
[24] Y. Nakamura, K. Oikawa, T. Kamiyama, E. Akiba, J. Alloys Compd. 316 (2001) 284–289.
[25] K. Kubo, H. Itoh, T. Takahashi, T. Kabutomori, Y. Nakamura, E. Akiba, Proceedings of 15th World Hydrogen Energy Conference, 2004.
[26] P.E. Blöchl, Phys. Rev. B 50 (1994) 17953–17979.
[27] X. Gonze, J.-M. Beuken, R. Caracas, F. Detraux, M. Fuchs, G.-M. Rignanese, L. Sindic, M. Verstraete, G. Zerah, F. Jollet, M. Torrent, A. Roy, M. Mikami, Ph. Ghosez, J.-Y. Raty, D.C. Allan, Comput. Mater. Sci. 25 (2002) 478–492.
[28] N.A.W. Holzwarth, A.R. Tackett, G.E. Matthews, Comput. Phys. Commun. 135 (2001) 329–347.
[29] E. Clementi, C. Roetti, At. Data Nucl. Data Tables 14 (1974) 177–478.
[30] Y. Shirai, K. Matsumoto, G. Kawaguchi, M. Yamaguchi, Mater. Sci. Forum 105–110 (1992) 1225–1228.
[31] Y. Kamimura, T. Tsutsumi, E. Kuramoto, Phys. Rev. B 52 (1995) 879–885.